JOURNAL OF MATERIALS SCIENCE **36** (2001) 3055–3059

Hydrothermal synthesis of $HNbWO_6$/MO series nanocomposites and their photocatalytic properties

JIHUAI WU*
Institute for Materials Physical Chemistry, Huaqiao University, Quanzhou 362011, China
E-mail: jhwu@hqu.edu.cn

SHU YIN
Institute for Chemical Reaction Science, Tohoku University, Sendai 980-8577, Japan

YU LIN, JIANMING LIN, MIAOLIANG HUANG
Institute for Materials Physical Chemistry, Huaqiao University, Quanzhou 362011, China

TSUGIO SATO
Institute for Chemical Reaction Science, Tohoku University, Sendai 980-8577, Japan

MO (M = Ni, Cu and Mn) or M_2O_3 (M = Fe and Cr) were intercalated into the interlayer of $HNbWO_6$ by hydrothermal reaction on $HNbWO_6$ with 1 M soluble $M(NO_3)_2$ or $M(NO_3)_3$ aqueous solution at 120°C.

1. Introduction

Photocatalytic reaction of layered nanocomposite semiconductors, such as splitting of water and reduction of carbon dioxide, has received special attention because of their possible application for the conversion of solar energy into chemical energy. Many studies have been carried out to enhance the photochemical activity of these catalysts. It is to be expected that the photoactivity of the semiconductor increases with the decrease of particle size since, in such a system, the distance which the photoinduced holes and electrons have to diffuse before reaching the interface decrease. Consequently, the holes and electrons can be effectively captured by the electrolyte in the solution [1]. Incorporation of semiconductor particles in the interlayer region of a lameller compound to form a nanocomposite consisting of host layers with ultrafine particles in the interlayer is a promising method for enhancing the photocatalytic activity of a semiconductor. As expected, the photocatalytic activities of incorporated semiconductors are much enhances when extremely small particles of Fe_2O_3, TiO_2 and CdS are intercalated into the interlayer of montmorillonite, layered double hydroxides, layered hydrous niobates and layered hydrous titanates [2–9].

It is considered that the preparation method and condition is an important element in enhancing photocatalytic activity of layered nanocomposite besides the choice of host and guest. In some case, semiconductor could not be effectively intercalated into the interlayer of layered compound owing to lacking of suitable methods. On the other hand, the structure and properties of nanocomposite depend on the methods and condition used in preparing the nanocomposite. In the present study, using hydrothermal method, new layered nanocomposites $HNbWO_6$/MO (M = Mn, Ni and Cu) and $HNbWO_6/M_2O_3$ (M = Cr and Fe) were synthesized and their photocatalytic activities were evaluated.

2. Experimental

2.1. Chemicals

Layered $HNbWO_6$ was prepared by proton exchange of $LiNbWO_6$ with 2 M HNO_3 at room temperature for 48 h with one intermediate replacement of the acid in between. Farinose $LiNbWO_6$ with particle size about $10^{-6} - 10^{-7}$ m was obtained by calcining stoichiometric mixture of Li_2CO_3, WO_3 and Nb_2O_5 at 800 °C in air for 24 h with one intermediate grinding in 12 h [10]. X-ray powder diffraction (shown in Fig. 1) proved the product to be single-phase $LiNbWO_6$ with a trirutile-type pattern [10].

$[Fe_3(CH_3COO)_7(OH)(H_2O)_2]NO_3$ was prepared as follows [2]: $Fe(NO_3)_3 \cdot 9H_2O$ (40 g) was added to 24 ml of ethyl alcohol and then reacted with 70 ml of acetic anhydride in ice bath by adding in small portions. The resulting precipitate was separated and dried without purification further.

Unsupported TiO_2 (Deggusa P-25) was commercially obtained and used without further purification. Unsupported Fe_2O_3 was prepared by adding a 1 M $Fe(NO_3)_3$ aqueous solution (50 ml) to a 5 M NH_3 aqueous solution (500 ml) at room temperature and the precipitate was washed with water until free of NH_3 and dried at 120 °C.

* Author to whom all correspondence should be addressed.

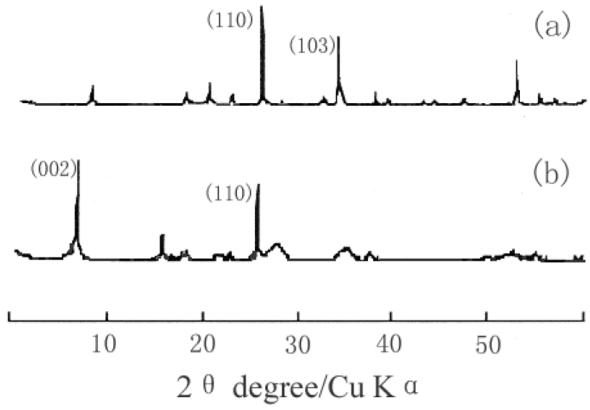

Figure 1 X-ray powder diffraction patterns of (a) trirutile $LiNbWO_6$, and (b) layered $HNbWO_6$.

2.2. Hydrothermal synthesis of $HNbWO_6$/MO (M = Mn, Ni and Cu) and $HNbWO_6/M_2O_3$ (M = Cr and Fe)

M^{2+} (M = Mn, Ni and Cu) or M^{3+} (M = Cr and Fe) ions were incorporated into the interlayer of $HNbWO_6$ by hydrothermal reaction of $HNbWO_6$ (4 g) with 1 M $M(NO_3)_2$ or $M(NO_3)_3$ aqueous solution (40 ml) in a 100 ml container at 120 °C for 12 h. After being filtered and washed with water, the precipitate was heated at 250 °C for 3 h so as to decompose any water remained in the interlayer of $HNbWO_6$. The samples obtained thus were designated as $HNbWO_6/Cr_2O_3$, $HNbWO_6$/MnO, $HNbWO_6/Fe_2O_3$, $HNbWO_6$/NiO and $HNbWO_6$/CuO.

2.3. Synthesis of $HNbWO_6/TiO_2^*$ and $HNbWO_6/Fe_2O_3^*$

TiO_2 acidic sol was obtained by adding titanium tetraisopropoxide to 1 M HCl solution with the TiO_2/HCl molar ratio of 0.25. $HNbWO_6$/n-$C_3H_7NH_2$ was prepared by stirring $HNbWO_6$ (1 g) in 50 ml of 20 Vol. % n-$C_3H_7NH_2$/n-heptane mixed solution under reflux at 50 °C for 72 h. $HNbWO_6$/n-$C_3H_7NH_2$ was added to TiO_2 acidic sol with the $TiO_2/HNbWO_6$ molar ratio of 20 and the suspension was continuous stirred for 6 h at room temperature so as to incorporate TiO_2 into the interlayer of $HNbWO_6$. After being filtered and washed with water, the specimen was dispersed in water and irradiated with UV light from a 450 W high-pressure mercury lamp at 60°C for 12 h so as to decompose any n-$C_3H_7NH_2$ remained in the interlayer of $HNbWO_6$. The sample obtained was designated as $HNbWO_6/TiO_2^*$.

Fe_2O_3 was incorporated into the interlayer of $HNbWO_6$ by irradiating the $[Fe_3(CH_3COO)_7(OH)(H_2O)_2]^+$ exchanged compound with UV light from a 450 W high-pressure mercury lamp at 50 °C for 12 h. The exchanged compound was obtained by ion-exchange reaction of $HNbWO_6$/n-$C_3H_7NH_2$ (2 g) with $[Fe_3(CH_3COO)_7(OH)(H_2O)_2]NO_3$ (25 g) in 500 ml water at 50 °C for 72 h. The sample obtained was designated as $HNbWO_6/Fe_2O_3^*$.

2.4. Analysis

The crystalline phases of the products were identified by X-ray diffraction (Rigaku Denki Geiger-flex 2013) using graphite monochromized Cu-K_α radiation. The chemical compositions of the samples were determined by TG-DTA analysis (Rigaku Denki TAS 200 TG-DTA) and by inductively coupled plasma atomic emission spectroscopy (Seiko SPS-1200A) after dissolving the samples in water by adding 0.1 g samples to HCl/HNO_3 (3 : 1) mixed solutions (120 ml) and boiling for 2 h. The band gap energies of the products were determined from the onset of diffuse reflectance spectra of the powders measured by using a Shimadzu Model UV-2000 UV-VIS spectrophotometer. The specific surface areas of samples were determined by nitrogen gas adsorption method (Quantachrome Autosorb-1).

2.5. Photocatalytic reaction

Photocatalytic reaction was carried out in a Pyrex reactor of 1250 ml capacity attached to an inner radiation type 450 W high-pressure mercury lamp. The inner cell had thermostat water flowing through a jacket between the mercury lamp and the reaction chamber. The inner cell was constructed with Pyrex glass that served to filter out the UV emission with $\lambda < 290$ nm from the mercury lamp. The light with $\lambda < 400$ nm was filtered out by flowing 1 M $NaNO_2$ solution between the mercury lamp and the reaction chamber. The photocatalytic activities of samples were determined by measuring the volume of hydrogen gas evolved with a gas burette when the suspensions of samples were irradiated.

3. Results and discussions

3.1. Intercalation of MO and M_2O_3 into the interlayer of $HNbWO_6$

Fig. 2 depicts the X-ray powder diffraction patterns of (a) $HNbWO_6$, (b) $HNbWO_6/TiO_2^*$, (c) $HNbWO_6/Cr_2O_3$, (d) $HNbWO_6$/MnO, (e) $HNbWO_6/Fe_2O_3^*$, (f) $HNbWO_6/Fe_2O_3$, (g) $HNbWO_6$/NiO and (h) $HNbWO_6$/CuO. The peak positions, corresponding to (110) of $HNbWO_6$, of samples (b)–(h) are almost the same as $HNbWO_6$ (a). But the position of (002) diffraction peaks of samples (a)–(f) are different and depend on the species in the interlayer. These results suggest that layered structures of $HNbWO_6$ are remained after intercalation of TiO_2, Cr_2O_3, MnO, Fe_2O_3, NiO and CuO although the interlayer distance changes. The gallery heights of $HNbWO_6/TiO_2^*$, $HNbWO_6/Cr_2O_3$, $HNbWO_6$/MnO, $HNbWO_6/Fe_2O_3^*$, $HNbWO_6/Fe_2O_3$, $HNbWO_6$/NiO and $HNbWO_6$/CuO determined by subtracting the $HNbWO_6$ layer thickness (0.76 nm) [11, 12] are 0.41, 0.31, 0.31, 0.29, 0.28, 0.29, and 0.30 nm respectively. Since the gallery height of $HNbWO_6$/MO and $HNbWO_6/M_2O_3$ are less than 0.31 nm, it is suggested that the thickness of intercalated layer are less than 0.5 nm which indicate the formation of nanocomposites. It is notable that the gallery height of $HNbWO_6/Fe_2O_3^*$ after the sample is dried at 250 °C for 3 h is close to those of $HNbWO_6/Fe_2O_3$,. It might be due to the same structure for $HNbWO_6/Fe_2O_3^*$ and $HNbWO_6/Fe_2O_3$ although different preparation methods are applied.

The UV-VIS diffuse reflection spectra of (a) $HNbWO_6$, (b) $HNbWO_6/TiO_2^*$, (c) $HNbWO_6/Cr_2O_3$,

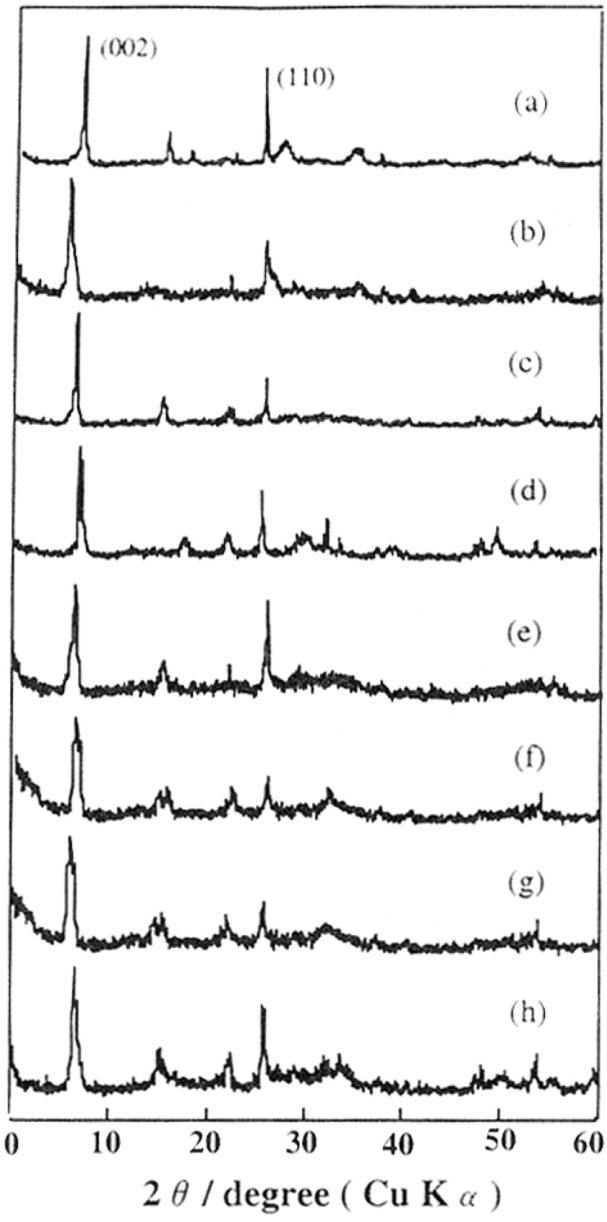

Figure 2 X-ray powder diffraction patterns of (a) $HNbWO_6$, (b) $HNbWO_6/TiO_2^*$, (c) $HNbWO_6/Cr_2O_3$, (d) $HNbWO_6/MnO$, (e) $HNbWO_6/Fe_2O_3^*$, (f) $HNbWO_6/Fe_2O_3$, (g) $HNbWO_6/NiO$ and (h) $HNbWO_6/CuO$.

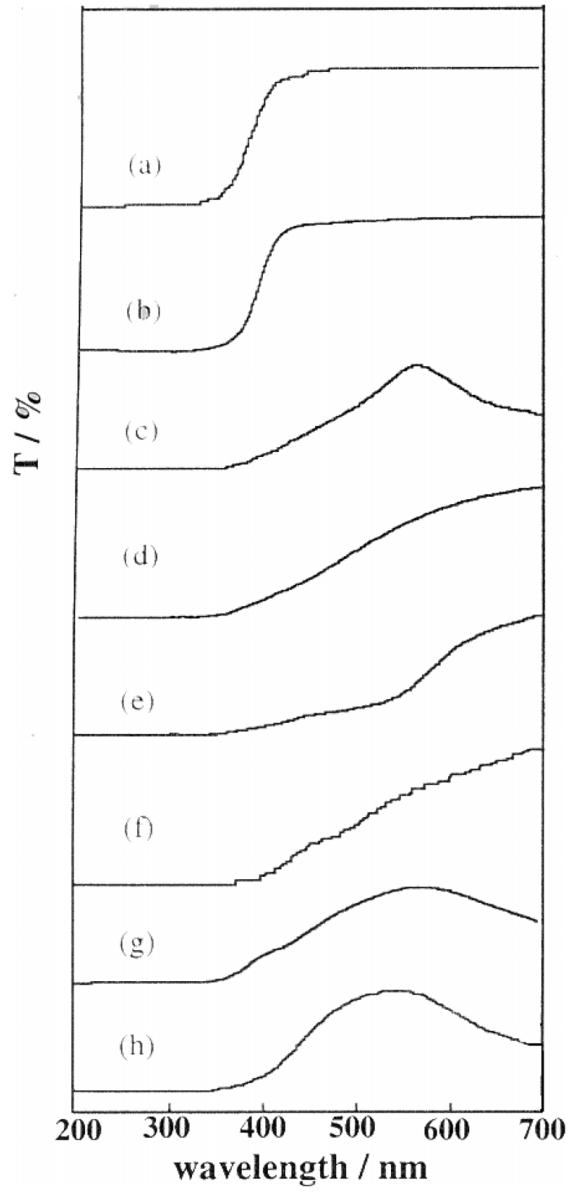

Figure 3 Diffuse reflection spectra of (a) $HNbWO_6$, (b) $HNbWO_6/TiO_2^*$, (c) $HNbWO_6/Cr_2O_3$, (d) $HNbWO_6/MnO$, (e) $HNbWO_6/Fe_2O_3^*$, (f) $HNbWO_6/Fe_2O_3$, (g) $HNbWO_6/NiO$ and (h) $HNbWO_6/CuO$.

(d) $HNbWO_6/MnO$, (e) $HNbWO_6/Fe_2O_3^*$, (f) $HNbWO_6/Fe_2O_3$, (g) $HNbWO_6/NiO$ and (h) $HNbWO_6/CuO$ are shown in Fig. 3. According to the formula $\Delta E = 1240/\lambda$ (nm), the band gap energy ΔE (eV) for each specimen can be calculated by its wavelength of adsorption edges λ (nm) on its inflexion of adsorption spectra. The spectra of $HNbWO_6$ and $HNbWO_6/TiO_2$ are almost same, indicating the onset at ca 400 nm (3.1 eV). On the other hand, other $HNbWO_6/MO$ and $HNbWO_6/M_2O_3$ nanocomposites show broad reflection spectra over 400–600 nm. The visible light absorption above 400 nm might be caused by the metal oxides incorporated. That different phenomena occurred on incorporated of TiO_2 and other metal oxides might be due to the different in band gap energies, i.e., the different in the band gap energies of TiO_2 and $HNbWO_6$ is not large, but that of other metal oxides and $HNbWO_6$ are large. Similar phenomena were also observed in $H_2Ti_4O_9/TiO_2$, $H_4Nb_6O_{17}/TiO_2$, $HTaWO_6/TiO_2$, $H_2Ti_4O_9/Fe_2O_3$, $H_4Nb_6O_{17}/Fe_2O_3$ and $HTaWO_6/Fe_2O_3$ systems [7, 8].

The gallery heights, amount of the metal elements intercalated, band gap energies and specific surface area of nanocomposites are summarized in Table I.

TABLE I Gallery height, element content, band gap energy and specific area of the samples

Sample	Gallery height** (nm)	Content(M) (Wt.%)	Band gap energy (eV)	Specific surface area ($m^2 \cdot g^{-1}$)
$HNbWO_6$	0.21		3.04	5.99
$HNbWO_6/TiO_2^*$	0.41	4.42	3.12	36.11
$HNbWO_6/Cr_2O_3$	0.31	3.01	2.20	14.70
$HNbWO_6/MnO$	0.31	3.27	2.26	13.97
$HNbWO_6/Fe_2O_3^*$	0.29	7.19	2.22	23.30
$HNbWO_6/Fe_2O_3$	0.28	5.65	2.04	16.94
$HNbWO_6/NiO$	0.29	3.69	2.17	18.87
$HNbWO_6/CuO$	0.30	5.09	2.30	13.65

**Gallery heights were detrermined after samples were dried at 250°C for 3 h.

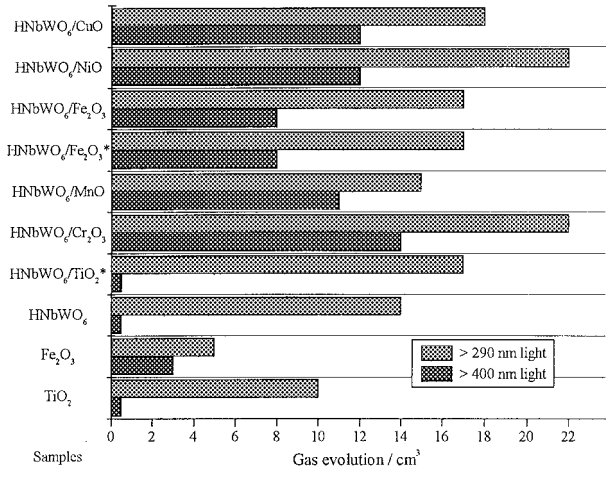

Figure 4 Volume of hydrogen gas produced from 1250 ml of Vol. 10% methanol solution containing 1 g of dispersed unsupported TiO_2, unsupported Fe_2O_3, $HNbWO_6$, $HNbWO_6/TiO_2^*$, (c) $HNbWO_6/Cr_2O_3$, $HNbWO_6$/MnO, $HNbWO_6/Fe_2O_3^*$, $HNbWO_6/Fe_2O_3$, $HNbWO_6$/NiO and $HNbWO_6$/CuO at 60 °C for 5 h under irradiation with $\lambda > 290$ nm and $\lambda > 400$ nm from a 450 W mercury arc.

The amount of the metal elements intercalated are 4.42, 3.01, 3.27, 7.19, 5.65, 3.69 and 5.09 Wt.% for $HNbWO_6/TiO_2^*$, $HNbWO_6/Cr_2O_3$, $HNbWO_6$/MnO, $HNbWO_6/Fe_2O_3^*$, $HNbWO_6/Fe_2O_3$, $HNbWO_6$/NiO and $HNbWO_6$/CuO nanocomposites, respectively. The higher Fe content in corporation of $Fe_2O_3^*$ than that in $HNbWO_6/Fe_2O_3$ indicate the ion exchange of Fe^{3+}, consequently incorporation Fe_2O_3 was promoted by the pre-expansion of the interlayer with $C_3H_7NH_3^+$. Owing to same reason, the specific surface of $HNbWO_6$/MO and $HNbWO_6/M_2O_3$ nanocomposites are $2 \sim 3$ times greater than that of $HNbWO_6$ which further indicate the intercalation of metal oxides and the formation of the MO and M_2O_3 pillars.

3.2. Photocatalytic properties

Fig. 4 shows volumes of hydrogen gas produced from 1250 ml of 10 Vol.% methanol solution containing 1 g of dispersed unsupported TiO_2, unsupported Fe_2O_3, $HNbWO_6$, $HNbWO_6/TiO_2^*$, $HNbWO_6/Cr_2O_3$, $HNbWO_6$/MnO, $HNbWO_6/Fe_2O_3^*$, $HNbWO_6/Fe_2O_3$, $HNbWO_6$/NiO and $HNbWO_6$/CuO at 60 °C for 5 h under irradiating with $\lambda > 290$ nm and $\lambda > 400$ nm from a 450 W mercury arc.

All samples show photocatalytic activities to evolve hydrogen gas under the irradiation with $\lambda > 290$ nm. The amount of hydrogen gas evolved increase in the sequence, unsupported Fe_2O_3 (5 ml) < unsupported TiO_2 (10 ml) < $HNbWO_6$ (14 ml) < $HNbWO_6$/MnO (15 ml) < $HNbWO_6/Fe_2O_3$ (17 ml) = $HNbWO_6/Fe_2O_3^*$ (17 ml) < $HNbWO_6/TiO_2^*$ (18 ml) = $HNbWO_6$/CuO (18 ml) < $HNbWO_6/Cr_2O_3$ (22 ml) = $HNbWO_6$/NiO (22 ml).

On the other hand, no hydrogen gas produced from TiO_2, $HNbWO_6$ and $HNbWO_6/TiO_2$ was observed under irradiation of visible light ($\lambda > 400$ nm), as expected from their ban gap energies (>3 eV). The photocatalytic activity of nanocomposites under visible light irradiation is in the order

$HNbWO_6/Cr_2O_3$ (14 ml) > $HNbWO_6$/CuO (12 ml) = $HNbWO_6$/NiO (12 ml) > $HNbWO_6$/MnO (11 ml) > $HNbWO_6/Fe_2O_3$ (8 ml) = $HNbWO_6/Fe_2O_3^*$ (8 ml) > unsupported Fe_2O_3 (3 ml).

The results suggested that the photocatalytic activities of Fe_2O_3 and TiO_2 are enhanced when they are intercalated in the interlayer of $HNbWO_6$. It indicates that the electrons and holes photoinduced from intercalated Fe_2O_3 can be effectively used for the reduction of water and oxidation of methanol, but the electrons and holes produced from unsupported Fe_2O_3 rapidly recombine. The depression of the recombination of electrons and holes might be due to electron transfer from Fe_2O_3 to host $HNbWO_6$. Similar results were observed in $H_4Nb_6O_{17}$, $H_2Ti_4O_9$ and $HTaWO_6$ systems [7, 8, 13].

It is notable that the photoactivity order of the above nanocomposites are different under irradiation with $\lambda > 290$ nm and $\lambda > 400$ nm. It might be due to the different optical characteristics and sensitivities of $HNbWO_6$/MO nanocomposites. It was also notable that the photocatalytic activity of $HNbWO_6/Fe_2O_3$ is almost the same as that of $HNbWO_6/Fe_2O_3^*$ under irradiation with $\lambda > 290$ nm or $\lambda > 400$ nm although different methods are applied to fabricate them. In view of the simplicity, convenience and start materials obtained easily for hydrothermal synthesis, it is suggested that hydrothermal synthesis methods are used to prepare layered nanocomposites more widely.

4. Conclusions

Based on above, the following conclusions may be drawn. (1) $HNbWO_6/Cr_2O_3$, $HNbWO_6$/MnO, $HNbWO_6/Fe_2O_3$, $HNbWO_6$/NiO and $HNbWO_6$/CuO nanocomposites were fabricated by hydrothermal reaction of $HNbWO_6$ with soluble $M(NO_3)_2$ or $M(NO_3)_3$ solution at 120 °C for 12 h followed by calcining samples at 250 °C for 3 h. (2) the height of MO and M_2O_3 pillars are less than 0.4 nm. The band gap energies of $HNbWO_6$/MO and $HNbWO_6/M_2O_3$ are less than 3 eV. (3) The photocatalytic activities of $HNbWO_6/TiO_2$ and $HNbWO_6/Fe_2O_3$ nanocomposites are superior to those of unsupported TiO_2 and Fe_2O_3, respectively. (4) $HNbWO_6/Cr_2O_3$, $HNbWO_6$/MnO, $HNbWO_6/Fe_2O_3$, $HNbWO_6$/NiO and $HNbWO_6$/CuO nanocomposites are capable of hydrogen gas evolution to the extent of 15–22 ml and 8–12 ml over 5 h following irradiation with $\lambda > 290$ nm and $\lambda > 400$ nm from a 450 W mercury arc in the presence of methanol as sacrificial holes acceptor.

Acknowledgements

This work was jointly supported by the National Natural Science Foundation of China (No. 50082003), the Provincial Natural Science Foundation of Fujian, China (No. E992001) and the Grant-in-Aid for Scientific

Research from the Ministry of Education, Science and Culture.

References

1. A. HAGFELDT and M. GRATZEL, *Chem. Rev*. **95** (1995) 49.
2. S. YAMANAKA, T. DOI and S. SAKO, *Mater. Res. Bull*. **19** (1994) 61.
3. O. ENENA and A. J. BARD, *J. Phys. Chem*. **90** (1986) 301.
4. H. MIYOSHI and H. YONEYAMA, *J. Chem. Soc. Faraday Trans*. **85** (1989) 1873.
5. H. YONEYAMA, S. HAGA and S. YAMANAKA, *J. Phys. Chem*. **93** (1989) 4833.
6. H. MIYOSHI, H. MORI and H. YONEYAMA, *Langmuir*. **7** (1991) 503.
7. T. SATO, Y. YAMAMOTO and S. UCHIDA, *J. Chem. Soc. Faraday Trans*. **92** (1996) 5089.
8. S. UCHIDA, Y. YAMAMOTO and T. SATO, *ibid*. **93** (1992) 3229.
9. T. SATO, K. MASAKI and K. SATO, *J. Chem. Tech. Biotechnol*. **67** (1996) 339.
10. V. BHAT and J. GOPALAKRISHNAN, *Solid State Ionics*. **26** (1988) 25.
11. R. P. SHANNON and C. P. PREWITT, *Acta Cryst*. **B25** (1961) 125.
12. E. CAZZANELLI, G. MARIOTTO and M. CATTI, *Solid State Ionics*. **53** (1992) 383.
13. J-H. WU, S. UCHIDA, Y. FUJISHIRO, S. YIN and T. SATO, *J. of Photochemistry and Photobiology A: Chemistry* **128** (1999) 129.

Received 2 July 1999
and accepted 20 December 2000